SUPPLEMENTARY INFORMATION of

RNA interactions drive structural and functional diversification of α-Synuclein fibrils

Jakob Rupert[1,#], Francesco di Palma[1,2], Alessio Colantoni[1,$], Antonia Intze[3], Maria Eleonora Temperini[3], Valeria Giliberti[3], Elsa Zacco[1,*] and Gian Gaetano Tartaglia[1,*]

1. RNA Systems Biology, Istituto Italiano di Tecnologia, Genoa, Via Enrico Melen, 83, 16152, Genoa, Italy
2. Department of Drug Science and Technology, University of Turin, Via Pietro Giuria, 9, 10125 Turin, Italy
3. Department of Physics, Sapienza University of Rome, Piazzale Aldo Moro 5, 00185 Rome, Italy
4. Center for Life Nano- & Neuroscience, Istituto Italiano di Tecnologia (IIT), Rome, Italy, Viale Regina Elena, 291, 00161 Roma Italy

[#] current affiliation: Institute for Biochemistry, Charité - Universitätsmedizin, Virchowweg 6, 10117 Berlin, Germany
[$] current affiliation: Departmental Faculty of Medicine, UniCamillus-Saint Camillus International University of Health Sciences, 00131 Rome, Italy

* correspondence to: elsa.zacco@iit.it, gian.tartaglia@iit.it

SUPPLEMENTARY METHODS

Inhibition mechanism analysis and fitting

The Dixon plot for aS fibril catalytic activity in the presence of increasing concentrations of RNA appeared to have a positive exponential curvature, indicating a complex mechanism such as parabolic inhibition. The data were fitted both to a simpler, empiric quadratic function (**Eq. 1**), and to a parabolic inhibition equation for two independent binding sites (**Eq. 2**):

(Eq. 1): $F(x) = A + Bx + Cx^2$

(Eq. 2): $\frac{1}{v_i} = \frac{1}{v_{max}}\left(1 + \frac{[RNA]}{K_{i,1}} + \frac{[RNA]^2}{(K_{i,1} \cdot K_{i,2})}\right)$

To compare the reliability of the parabolic mechanism fit compared to the hyperbolic mechanism, data were further fitted to the mechanistic hyperbolic equation for 2 independent binding sites (Eq. 3):

(Eq. 3): $\frac{1}{v_i} = \frac{1}{v_{max}} \frac{\left(1 + \frac{[RNA]}{K_{i,1}}\right)\left(1 + \frac{[RNA]}{K_{i,2}}\right)}{\left(1 + F_{ESI}\right)}$

Sequence analysis

A rough overall analysis of the aS fibril-bound transcriptome was performed by looking at nucleotide composition, structural propensity and presence of significant motifs to complement and expand on the k-mer analysis (**Main Fig. 6**). RNA structural propensity was probed with the CROSS tool using the Global score model (1) . To produce the final RNA propensity score, the number of nucleotides with a positive CROSS score was normalised by transcript length. Motif analysis was performed with the XSTREME tool from MEME suite(2). Motif enrichment was performed both against abundance- and length-matched controls using pre-compiled RNA motif libraries from literature (3). Only motifs with a length between 6 and 15 nucleotides and an e-value below 0.1 were taken into consideration. All the results were imported into Python for data wrangling and plotting.

Supplementary Figures

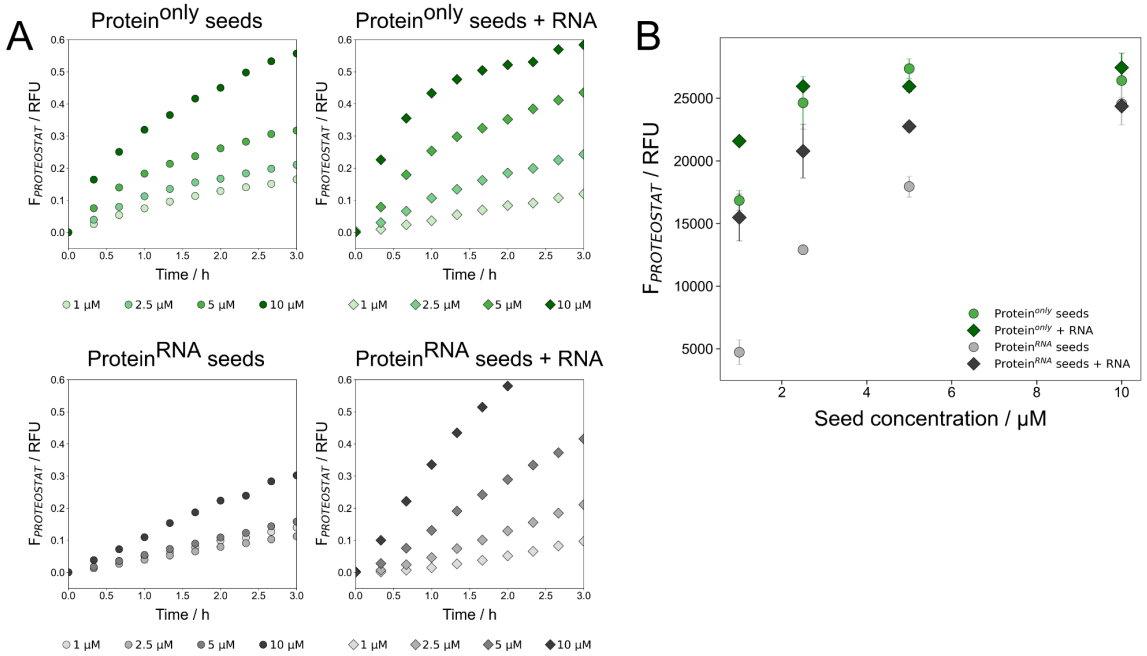

Supplementary figure 1. (*A*) Early-stage aggregation kinetics of 50 µM aS at varying seed concentrations and in the presence or absence of RNA clearly show the effect of different seed type, as well as the addition of RNA on the aggregation of aS. Protein^{RNA} seeds have a much lower seeding capacity compared to protein^{only} seeds and only start effectively accelerating the aggregation kinetics at 10 µM concentration. The presence of RNA significantly accelerates the kinetics in both cases. (*B*) Peak Proteostat^{TM} fluorescence signal at varying seed concentrations roughly corresponds to the amount of aggregated species, providing an estimate of the seeding ability of different seed species. Protein^{RNA} seeds have the overall lowest peak fluorescence, further indicating their lower seeding ability compared to protein^{only} seeds as already demonstrated by the slower aggregation kinetics.

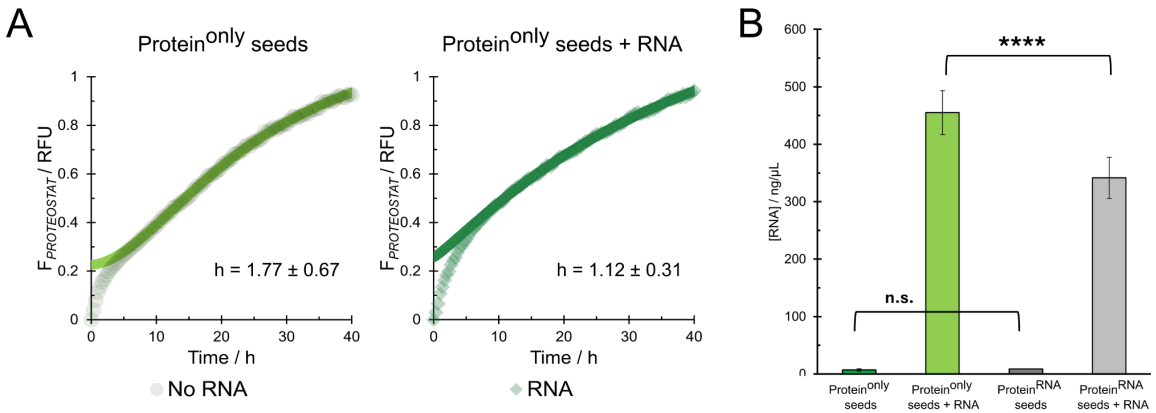

Supplementary figure 2. (*A*) Fitting the later exponential stage of fibril growth for protein^{only}-seeded kinetics with the sigmoid equation (see **Materials and Methods**) results in Hill coefficients (h) of 1.12 ± 0.31 in the presence and 1.77 ± 0.67 in the absence of RNA ($p = 0.012$, $N = 8$, two-way Student t-test). This indicates an absence of secondary processes in the presence of RNA and potentially implies that while RNA increases the elongation rate, it also reduces the surface-mediated secondary nucleation processes. (*B*) Soluble RNA quantification after aggregation shows a significant decrease for reactions, seeded with protein^{RNA} seeds ($p < 0.001$, $N = 8$, Student t-test).

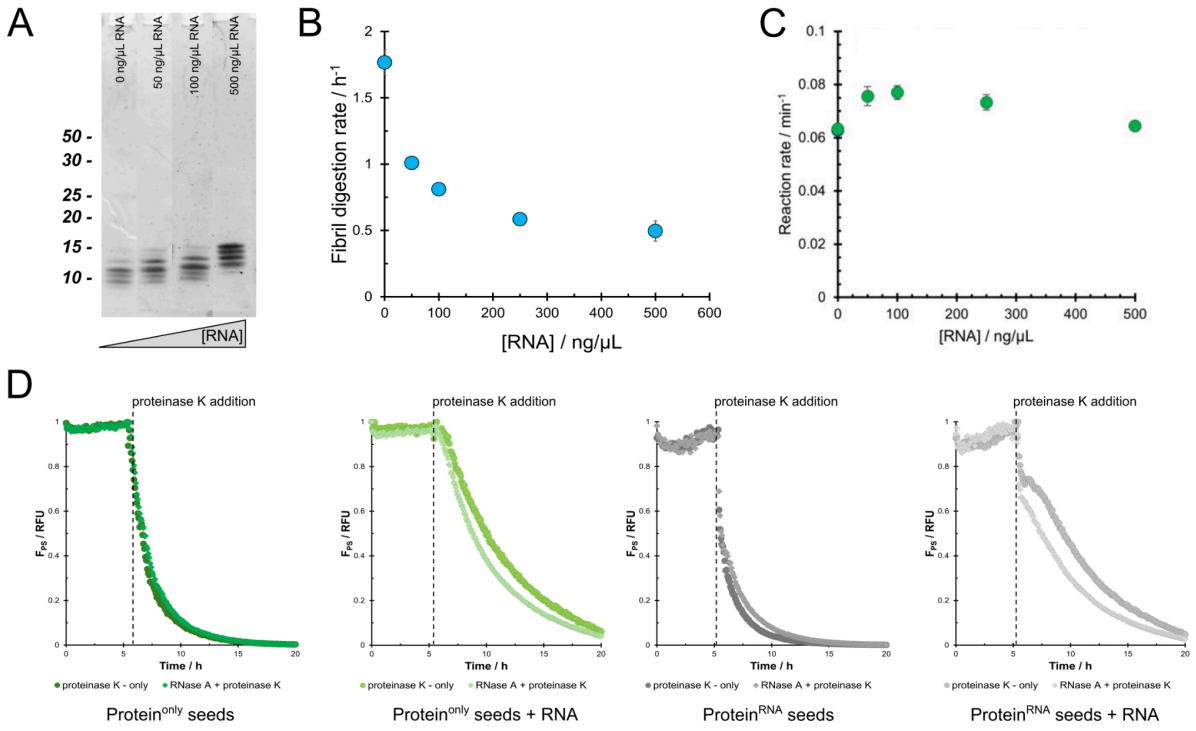

Supplementary figure 3. (*A*) SDS-PAGE gel analysis reveals differences in the degradation of aS aggregates by 0.5 µg/mL pK when incubated with increasing concentrations of RNA. (*B*) aS fibril degradation rate with pK decreases exponentially with increasing RNA concentrations. (*C*) Degradation of the enzymatic substrate pNPA by proteinase K in the presence of RNA. The rate of pK activity does not decrease at higher RNA concentrations, indicating that RNA does not inhibit pK activity directly. (*D*) Treatment of aS fibrils with RNase A for 5 h at 37 °C (lighter coloured traces) does not result in changes in fluorescence intensity with respect to controls (darker coloured traces), implying that RNase A itself does not affect the fibrils integrity. In contrast, RNase A-treated samples show a faster decay of fluorescence upon pK addition in the case of fibrils aggregated with RNA. No change is observed for fibrils, aggregated in the absence of RNA.

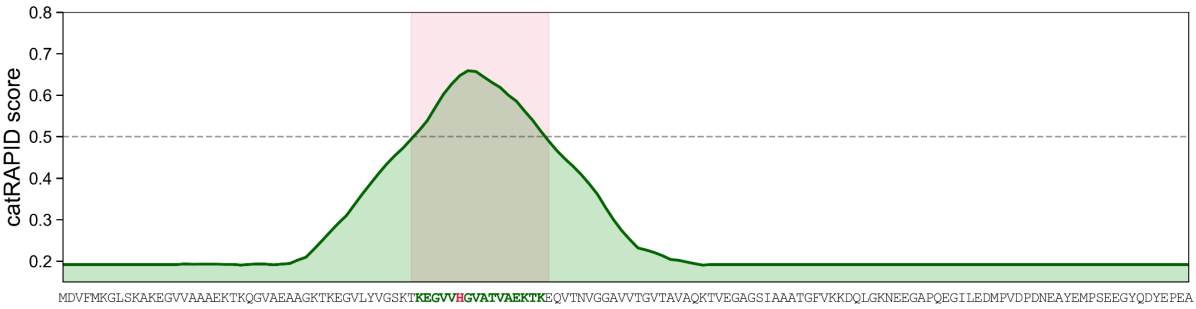

Supplementary figure 4. *cat*RAPID signature profile of aS with the position of His50 highlighted with the vertical line in the predicted area with the highest RNA binding propensity. The vertical line marks the z-score threshold of 0.5, indicative of significant RNA-binding propensity, with the coloured area highlighting the corresponding residues of aS. His50, the residue presumed to be involved in the fibril catalytic activity, is highlighted in red.

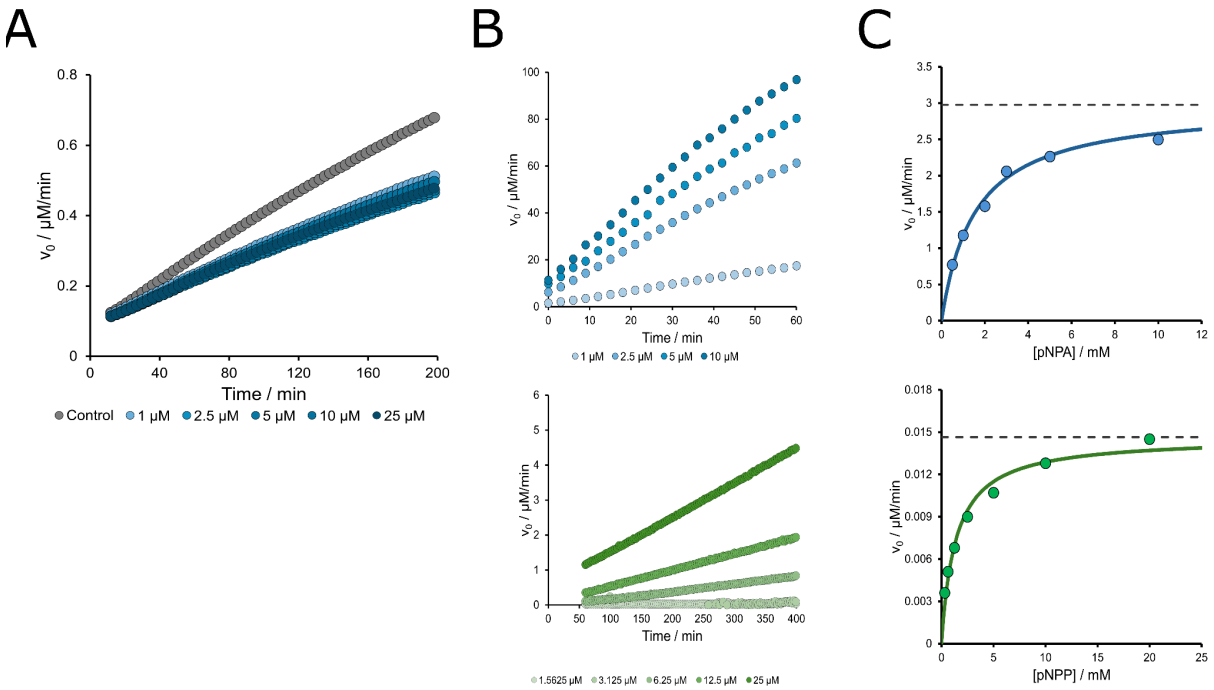

Supplementary figure 5. (*A*) Monomeric aS at a range of concentrations does not contribute to any pNPA cleavage compared to control (assay buffer), indicating that any observed catalytic activity is due to fibrillar aS. The rise in signal is due to water hydrolysis of pNPA, while pNPP does not hydrolyse in water and no increase in signal can be observed (data not shown). (*B*) Increasing concentrations of aS fibrils contribute to the increase in catalytic activity, further confirming the catalytic activity of aggregated aS. The initial velocities obtained from pNPA (top) and pNPP (bottom) cleavage at different substrate concentrations can be plotted to determine the catalysis parameters via the Michaelis-Menten plot (*C*). The Michaelis-Menten constant K_M is determined as the concentration of the substrate at 50 % maximum reaction velocity and reflects the affinity of the enzyme to the substrate as outlined in **Materials and Methods**.

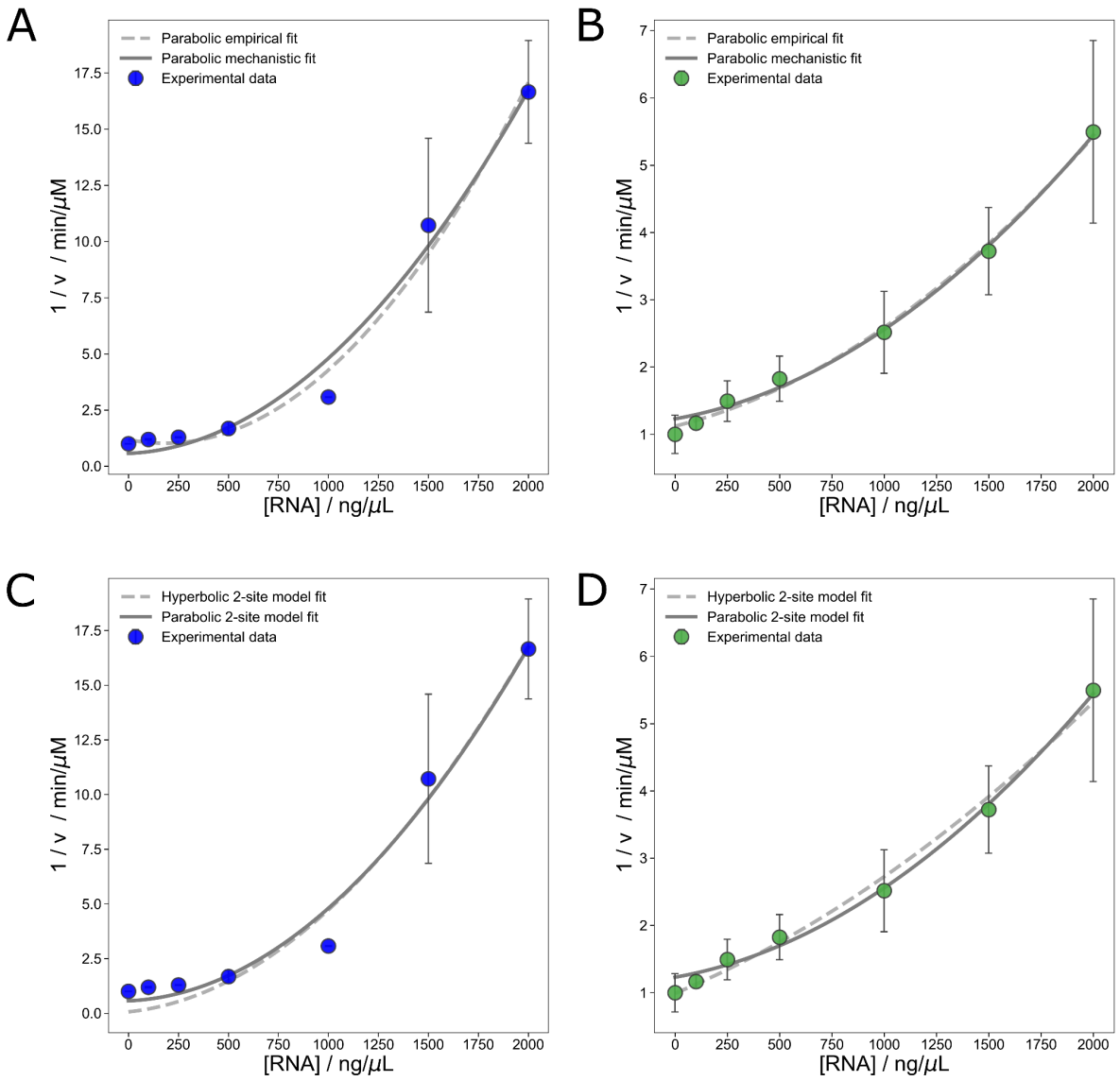

Supplementary figure 6. Plotting the inverse initial velocities against the inhibitor concentration such as RNA, the Dixon plot can provide insight into the mechanism of inhibition (**Supplementary Methods**). Both for pNPA (*A*) and pNPP (*B*), the exponentially increasing inverse velocities suggest either a parabolic or complex hyperbolic mechanism with multiple independent sites. The fits for both models were compared for pNPA (*C*) and pNPP (*D*) and while the parabolic two-site inhibition model produced a lower residual sum of squares (RSS) than the hyperbolic two-site model, the improvement was not statistically significant (F-test, $p > 0.05$).

A

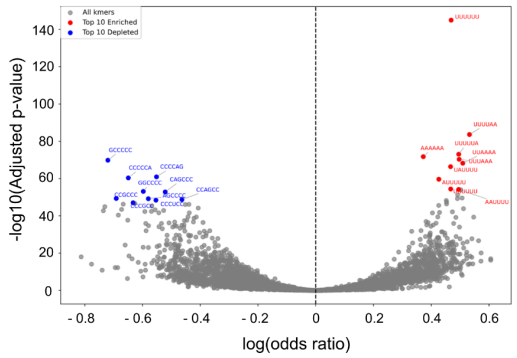

Top 10 depleted motifs					Top 10 enriched motifs				
Rank	RNA motif	Odds Ratio	p-value	Adjusted p-value	Rank	RNA motif	Odds Ratio	p-value	Adjusted p-value
1	GCCCCC	0.486672	2.13E-73	1.46E-70	1	UUUUUU	1.598182	2.5E-149	1E-145
2	CCCCAG	0.575964	2.58E-64	1.17E-61	2	UUUUAA	1.702847	1.13E-87	2.31E-84
3	CCCCCA	0.522386	1.08E-63	4.42E-61	3	UUUUUA	1.640622	6.5E-77	8.88E-74
4	GGCCCC	0.550267	2.81E-56	7.67E-54	4	AAAAAA	1.451145	1.72E-75	1.76E-72
5	CAGCCC	0.59366	5.84E-56	1.49E-53	5	UUUAAA	1.643087	5.76E-74	4.72E-71
6	CCGCCC	0.501011	2.14E-52	4.61E-50	6	UUAAAA	1.663836	9.98E-72	5.84E-69
7	AGCCCC	0.559904	3.23E-52	6.29E-50	7	UAUUUU	1.59495	8E-70	4.1E-67
8	CCAGCC	0.629117	9.84E-52	1.83E-49	8	AUUUUU	1.531416	6.21E-63	2.31E-60
9	CCCUCC	0.574822	2.19E-51	3.91E-49	9	UGUUUU	1.595677	1.2E-57	4.1E-55
10	CCCGCC	0.531113	6.07E-50	9.56E-48	10	AAUUUU	1.640074	2.22E-57	6.99E-55

B

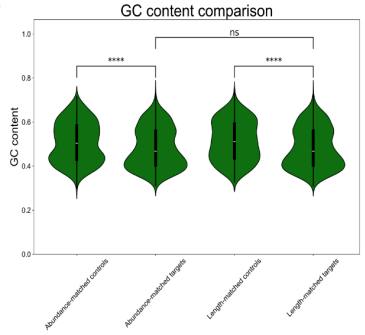

C

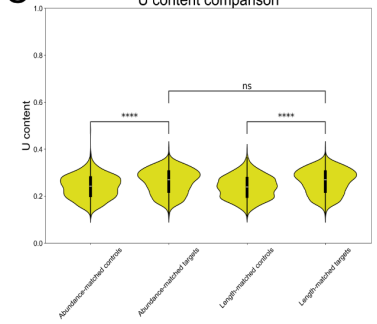

D

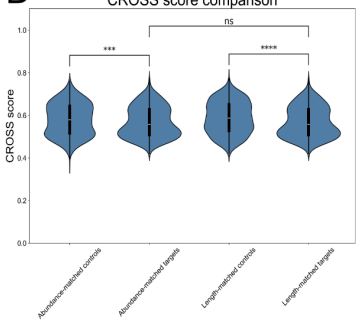

E

Abundance-matched controls

Motif ID	Motif sequence	N of sites	Motif e-value
MEME-1	UUUUUUUUUUUUUUU	620	1.3E-24
MEME-2	AAUWUUUDUAUUUUU	324	2.40E-08
STREME-1	GGCUCUUUUCAGUG	231	0.048
STREME-2	UUUAAAAUGAG	180	0.054
STREME-3	UUUUUUUUUAG	323	0.071

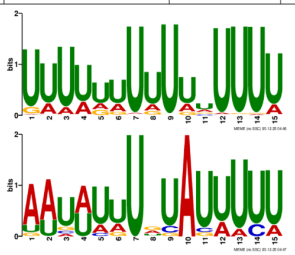

F

Length-matched controls

Motif ID	Motif sequence	N of sites	Motif e-value
MEME-1	UUUUUUUUUUUUUUU	435	1E-18
MEME-2	SCSGCGSCSSSGGCS	791	3.50E-07
STREME-1	CGCCGCCG	926	1.90E-04
STREME-2	GCGGCCGCG	720	4.80E-04
STREME-3	CGCGCG	851	8.50E-04
STREME-4	UUAAUAAA	890	8.30E-03
STREME-5	UAUUUUUAAACUUA	213	0.02
STREME-6	GCUCUUUUCAGAGCC	57	0.022
STREME-7	UUUUUUCUUUUA	350	0.025

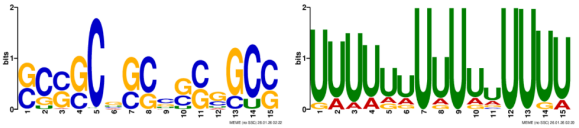

Supplementary figure 7. Analysis of transcripts, enriched in the coaggregation fraction of aS fibrils. (A) Results of the hexamer enrichment analysis comparing human transcripts specifically bound by Protein^{RNA} fibrils with a length-matched control set of RNAs (see Materials and Methods). Left panel: Volcano plot showing the log(Odds Ratio) versus –log$_{10}$(adjusted p-value). The 10 most enriched and 10 most depleted hexamers, selected based on adjusted p-value, are highlighted in red and blue, respectively. Right panel: Table reporting the sequence, Odds Ratio, p-value, and adjusted p-value for these 20 hexamers. Motif enrichment was assessed using the chi-square test, and p-values were corrected for multiple testing using the Benjamini–Hochberg procedure. (B,C) The comparison of fibril-enriched RNA with their abundance- and length-matched controls reveals a significantly lower GC-content in the RNA, extracted from the fibrils ($p < 10^{-10}$, Mann-Whitney U-test) and a higher uracil content ($p < 10^{-10}$, Mann-Whitney U-test) in accordance with the k-mer analysis of transcripts. (D) Analysis of RNA structural propensity with CROSS consequently results in significantly lower scores compared to both abundance- ($p = 3.54x10^{-4}$, Mann-Whitney U-test) and length-matched controls ($p < 1x10^{-9}$, Mann-Whitney U-test). (E) These results are confirmed by XSTREME analysis for motif enrichment, with U-rich motifs by far the most significantly enriched compared to abundance-matched controls. (F) Comparison to length-matched controls also reveals another enrichment of GC-rich motifs together with U-rich motifs. These tend to be shorter than the U-rich ones, indicating a wider preference for binding motifs could exist.

Supplementary Tables

Supplementary table 1. Kinetic parameters of catalytic activity of aS fibrils, compared to values reported in literature (4) . The values reported have been calculated from parameters, obtained in 7 (pNPP) and 3 independent experiments (pNPA). The fibrils were prepared freshly for each individual experiment (see Materials and Methods).

Supplementary Table 2. RNA species differentially associated with aS fibrils identified by RNA-sequencing.

This table summarizes transcripts selectively bound or incorporated into aS fibrils as determined by differential enrichment analysis (sleuth Wald test, $q < 0.05$, log2 fold-change > 0.58). It includes the following categories:

Input – The complete reference transcriptome used as background for all enrichment analyses, containing all detected RNAs above the FPKM threshold.

Coaggregated targets – RNAs significantly enriched in fibrils formed in the presence of RNA. These represent transcripts incorporated into the fibril structure during coaggregation.

Coaggregated ctrls (length) – length-matched RNAs not enriched in coaggregation ($q > 0.25$), serving as the background/control set matched for comparison.

Coaggregated ctrls (abundance) – abundance-matched RNAs not enriched in coaggregation ($q > 0.25$), serving as the background/control set matched for comparison.

References

1. R. Delli Ponti, S. Marti, A. Armaos, G. G. Tartaglia, A high-throughput approach to profile RNA structure. *Nucleic Acids Res.* **45**, e35 (2017).
2. C. E. Grant, T. L. Bailey, XSTREME: Comprehensive motif analysis of biological sequence datasets. *Bioinformatics* (2021).
3. D. Ray, *et al.*, A compendium of RNA-binding motifs for decoding gene regulation. *Nature* **499**, 172–177 (2013).
4. I. Horvath, P. Wittung-Stafshede, Amyloid fibers of α-synuclein catalyze chemical reactions. *ACS Chem. Neurosci.* **14**, 603–608 (2023).